Correlated memory resistor in epitaxial NdNiO3 heterostructures with asymmetrical proton concentration

Chadol Oh, Seungyang Heo, Hyun M. Jang, and Junwoo Son

Citation: Applied Physics Letters **108**, 122106 (2016); doi: 10.1063/1.4944842
View online: http://dx.doi.org/10.1063/1.4944842
View Table of Contents: http://scitation.aip.org/content/aip/journal/apl/108/12?ver=pdfcov
Published by the AIP Publishing

Correlated memory resistor in epitaxial $NdNiO_3$ heterostructures with asymmetrical proton concentration

Chadol Oh,[1] Seungyang Heo,[2] Hyun M. Jang,[2] and Junwoo Son[1,a)]
[1]*Department of Materials Science and Engineering, Pohang University of Science and Technology (POSTECH), Pohang 790-784, Republic of Korea*
[2]*Division of Advanced Materials Science, Pohang University of Science and Technology (POSTECH), Pohang 790-784, Republic of Korea*

(Received 21 October 2015; accepted 13 March 2016; published online 23 March 2016)

The electronic devices using correlated transition metal oxides are the promising candidates to overcome the limitation of the current electronics due to the rich electronic phases and the extreme sensitivities. Here, we report proton-based resistive switching memory that uses correlated oxides, i.e., epitaxial $NdNiO_3$ heterostructure with asymmetrical concentration of protons (H^+) to obtain multilevel states. By designing such metal-$NdNiO_3$-metal device structures with asymmetrical proton concentration, we demonstrate that the correlated oxides exhibit resistive switching by ionic transport of protons at the metal-hydrogenated $NdNiO_3$ (H-NNO) interface. This finding will guide the development of energy-efficient switching devices for non-volatile memory and neuromorphic applications. © *2016 AIP Publishing LLC*. [http://dx.doi.org/10.1063/1.4944842]

Correlated transition metal oxides have attracted considerable attention due to a remarkable variety of functionalities that originate from the strong correlations between the localized transition metal valence *d* electrons.[1,2] One representative functionality is abrupt Mott phase transition under external stimuli, e.g., metal-insulator transition (MIT), in correlated electron systems.[3] The unique phenomenon observed in these materials exhibits sensitivities that cannot be achieved by using conventional semiconductor alone, and thus the control of the rich electronic phases in the correlated oxides may open up an important arena for future electronics to overcome the limitation of current electronic devices.[4–10] Electronic devices that exploit the Mott transition have been conceptually suggested and experimentally demonstrated.[6–10] Correlated devices that utilize MIT materials achieve current drive and subthreshold slope that exceed those of current electronic switches,[6,10] and also realize unique device characteristics, such as charge gain,[6] collective carrier delocalization,[7] and synaptic analogue states.[9]

Among a variety of correlated oxides, rare-earth nickelates ($RNiO_3$) are a well-recognized class of transition-metal oxides that undergo sharp MIT at transition temperature.[11] In addition to temperature, the MIT of $RNiO_3$ can be dramatically modulated by various methods, including strain,[12,13] pressure,[14,15] confinement,[2,16,17] stoichiometry,[18,19] and electrostatic doping.[20,21] Among the several efforts to modulate the strong correlation of $RNiO_3$, it has been recently demonstrated that the resistivity of $SmNiO_3$ (SNO) thin films can be reversibly modulated up to eight orders of magnitude by proton (H^+) doping, thereby realizing a colossal MIT.[22,23] A giant resistivity modulation of SNO by proton doping is caused by the extreme sensitivity of electrical property to atomic defects in correlated systems. Therefore, this facile metal-to-insulator transition by proton doping can be utilized to realize extremely sensitive electronic devices that use correlated material systems.

In this Letter, we report proton-based resistive switching with multilevel states in a two-terminal epitaxial $NdNiO_3$ heterostructure device with asymmetrical proton concentration. We used selective proton doping to design these asymmetrical metal-$RNiO_3$-metal device structures and realized proton-based memory resisters with consistent clockwise interface-type resistive switching and protonic analog synaptic features. Because positively charged proton ions have higher ion mobility than that of oxygen ions (O^{2-}) in a potential wall of the oxide lattice, and because resistance can be modulated sensitively by asymmetrical proton doping in $RNiO_3$, use of this protonic memory resistor in $RNiO_3$ can potentially improve the switching power and speed compared to typical memristors based on the migration of oxygen ions.

Before device fabrication, epitaxial $NdNiO_3$ (NNO) films were grown on (001)-oriented $LaAlO_3$ (LAO) substrates by pulsed laser deposition (PLD). High-quality NNO films on LAO substrates were coherently grown up to 25 nm under compressive strain as reported previously.[21,24] Reciprocal space mapping performed around pseudocubic $(\bar{1}03)$ diffraction peak reveals that the NNO is fully strained along the in-plane direction on LAO substrate (Fig. S1(b)[25]). Atomic force microscopy results confirmed that the films were atomically smooth with unit cell step height (Fig. S2(a)[25]). The "untreated" NNO thin films were metallic with measured room-temperature (RT) resistivity ~357 $\mu\Omega$ cm, which is consistent with that of other compressively strained NNO thin films with good stoichiometry (Fig. S2(b)).[18,21,24,25]

To inject proton into the NNO lattice, we employed catalytic "spillover" method with Pt electrodes as a catalyst, which dissociates H_2 into atomic hydrogen at the triple phase boundary (Pt-NNO-H_2).[22] To establish asymmetrical proton concentration that differed between the two Pt electrodes, they were separately deposited between successive

a)jwson@postech.ac.kr

proton-injection processes as described in Fig. 1(a). First, 50-nm-thick Pt electrodes with different areas ($50 \times 50\ \mu$m to $210 \times 210\ \mu$m), which are referred to as H-Pt hereafter, were sputtered on an epitaxial NNO layer through a shadow mask. Then, the samples were annealed in forming gas (H_2/Ar = 5/95) at 100 °C for atomic hydrogen to diffuse selectively into the NNO lattice right under the H-Pt electrodes without increasing oxygen deficiency. Finally, other Pt electrodes with $300 \times 300\ \mu$m size, denoted as NH-Pt hereafter, were also deposited $\sim 700\ \mu$m away from the H-Pt electrodes.

The process (Fig. 1(a)) was intended to incorporate proton into the NNO layers only under the H-Pt electrodes, and not under the NH-Pt. Because annealing temperature ($\sim$100 °C) under forming gas is low enough that lateral diffusion of proton is weak in our asymmetrical devices, unlike the previous reports on the proton doping of RNiO$_3$ (Fig. S6), it is difficult to recognize the change of color contrast around H-Pt electrodes (Fig. 1(b), inset). However, the NNO

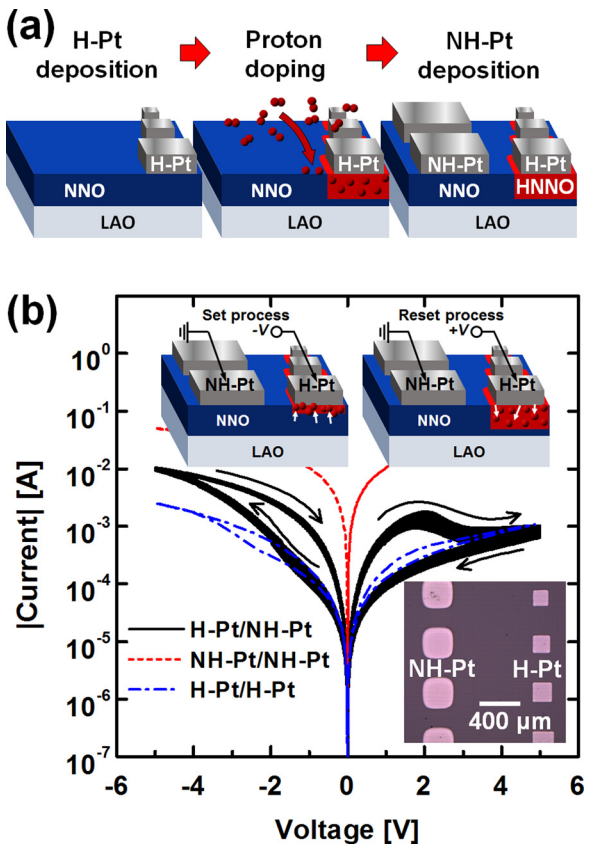

FIG. 1. (a) Schematic diagram of device fabrication process for asymmetrical proton concentration, which consists of H-Pt deposition, proton doping, and NH-Pt deposition. Through this process, atomic hydrogen enables to diffuse selectively into NNO lattice (H-NNO) right under H-Pt electrodes. (b) Two-terminal current-voltage (IV) characteristics of our devices with differently processed Pt electrodes: NH-Pt/NNO/NH-Pt (red line), "symmetrical" H-Pt/NNO/H-Pt (blue line), and "asymmetrical" H-Pt/NNO/NH-Pt (black line). The voltage-induced resistance modulation in "symmetrical" devices is significantly suppressed compared to that in "asymmetrical" devices. A bias voltage was always applied to H-Pt electrode and the NH-Pt electrode was grounded to ensure the switching direction in "asymmetrical" H-Pt/NNO/NH-Pt devices. The inset shows plain-view optical microscopy (OM) image of our protonic memory resistors with NNO epitaxial layers. Unlike OM in Ref. 22, it is difficult to recognize the change of H^+-induced color contrast around H-Pt electrodes in our device due to the low annealing temperature (100 °C).

layer around the H-Pt electrodes, i.e., hydrogenated NNO layer (H-NNO), is expected to be electrically and optically insulating. To confirm that proton doping in our NNO epitaxial films affects phase transition, our NNO samples with regular Pt patterns were annealed under the forming gas at 200 °C, which allows proton doping in the entire area of the samples. The resistivity of our H-NNO was sensitively increased up to 10^6 times compared to the metallic NNO layer (Fig. S3(a)[25]), indicating metal-to-insulator transition by proton doping in NNO. The resistivity of H-NNO decreases slowly down to one order of magnitude and then still hold the same order of magnitude even after 4 days (Fig. S4[25]). It was previously claimed that the giant resistivity increase has been attributed into the electronic effect, i.e., bandgap opening by injecting electrons to the e_g orbitals and converting Ni^{3+} to Ni^{2+}.[22] Indeed, Ni^{3+} $3d$ peak is suppressed and Ni^{2+} $3d$ peak appears in our H-NNO films after hydrogenation in X-ray absorption spectroscopy (XAS, Fig. S5[25]), indicating that Ni valence change by proton doping is responsible for the following proton-based resistive switching in our devices.

The effect of proton treatment on our device can be sensitively observed from the following electrical measurements. Fig. 1(b) shows the comparison of the I-V characteristics of two symmetrical devices (NH-Pt/NNO/NH-Pt and H-Pt/NNO/H-Pt) and one asymmetrical device (H-Pt/NNO/NH-Pt). The current was measured using two point probe by sweeping voltage from 0 V to −5 V, then back to 0 V, and then from 0 V to +5 V, and finally back to 0 V. Due to the metallic nature of NNO thin films at room temperature, NH-Pt/NNO/NH-Pt devices show Ohmic-like linear I-V characteristics without any memory effect; this characteristic confirms that the hydrogen treatment did not affect the catalyst-free NNO layer under NH-Pt electrodes. In contrast, H-Pt/NNO/H-Pt devices show Schottky-like nonlinear I-V characteristics with low current and negligible memory effect with small IV hysteresis; this behavior is ascribed to the formation of an insulating NNO barrier induced by proton doping (H-NNO) near the H-Pt electrodes, presumably the formation of back-to-back Schottky junction barriers at two H-Pt/H-NNO interfaces.

Interestingly, H-Pt/NNO/NH-Pt devices with asymmetrical electrodes consistently show "clockwise" bipolar resistive switching in I-V curves without a forming process: When the negative "set" voltage is applied to H-Pt, current level increases smoothly and the devices switch from high resistance state (HRS) to low resistance state (LRS). At the positive "reset" voltage, the devices switch back to HRS. Moreover, the resistances of the device at both LRS and HRS are inversely proportional to the electrode area (Fig. 2(a), inset); this relationship clarifies that the resistive switching occurs at the interface between H-Pt and H-NNO, not at the local filaments. Remarkably, it should be pointed out that this clockwise resistive switching is rarely observed in typical interface-type resistive switching devices that exploit migration of negatively charged oxygen ions. The clockwise I-V hysteresis in our asymmetrical devices may be due to the movement of (positively charged) hydrogen ions.[26,27] The voltage-induced resistance modulation in symmetrical devices is significantly suppressed compared to that in asymmetrical devices because the protons at two interfaces (H-Pt/H-NNO) simultaneously

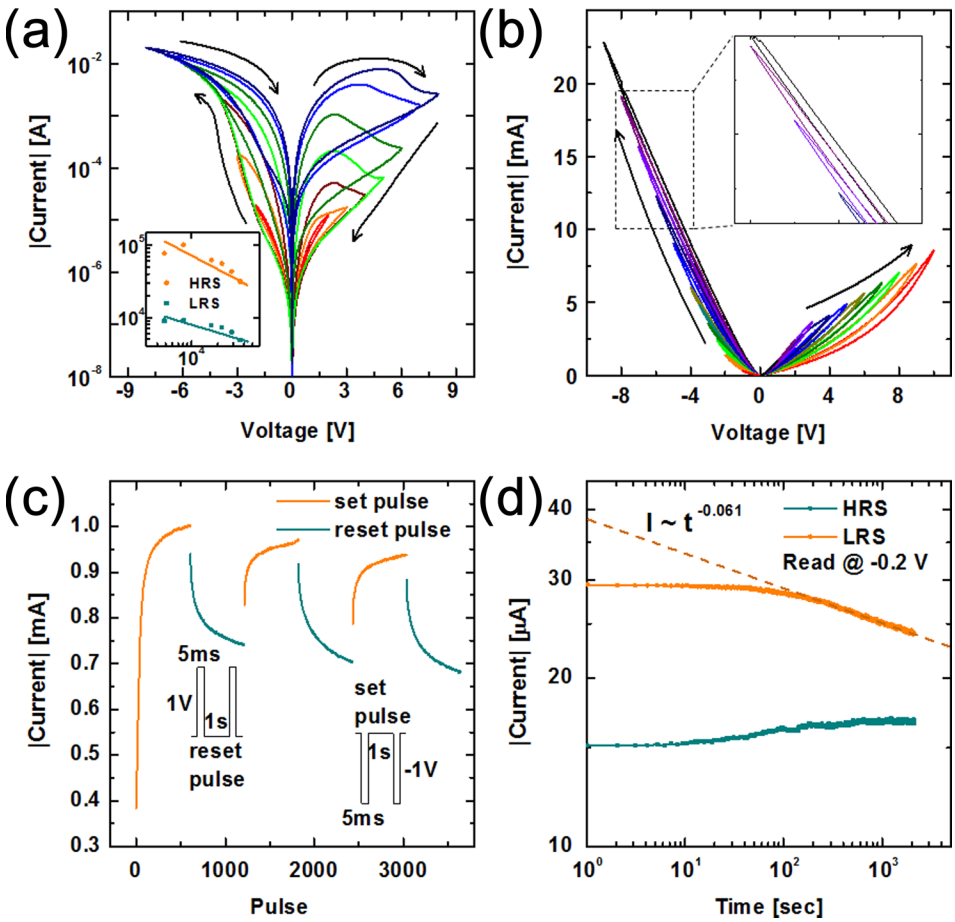

FIG. 2. (a) IV characteristics of the asymmetrical device (H-Pt/NNO/NH-Pt) with gradually increasing the sweeping width of voltages (from $-2\,V \le V \le 2\,V$ to $-8\,V \le V \le 8\,V$). The inset shows resistances at HRS and LRS in devices with various cell areas. (b) IV characteristics with different set and reset voltages applied to H-Pt electrodes repeatedly with sweep widths of $-1.0\,V$ to $-9.0\,V$ in the negative direction and $+1.0\,V$ to $+10.0\,V$ in the positive direction, respectively. The inset shows the enlarged plot in the range of the negative bias of the IV curves. (c) Conductance modulation by iterative small voltage pulses with 600 potentiating (or set) pulse sequences first and then the successive 600 depressing (or reset) pulse sequences. The voltage level and duration in pulses were set to $\pm 1\,V$ and 5 ms, respectively, with a 1 s interval. (d) Retention test of our protonic memory resistors. The current was measured at $-0.2\,V$ for HRS and LRS.

migrate toward the direction of electric field in symmetrical devices, which leads to smaller LRS/HRS switching ratio.

Repetitive hysteretic behavior was observed by applying the voltage sweep more than 100 times in asymmetrical devices; this result confirms that the resistive switching is consistent and repeatable. Because the hydrogenation process was performed in the absence of NH-Pt, the proton was introduced vertically and laterally in NNO only below (or near) the H-Pt electrodes during forming gas annealing. Therefore, proton intercalation seems to contribute to the resistive switching behavior in these asymmetrical devices. Although the distance between H-Pt and NH-Pt is long ($\sim$700 μm), the set and reset voltages $\sim \pm 5\,V$ induce bipolar resistive switching; this result indicates that the voltage drop and resistive switching occur only near the interface between H-Pt and NNO, and thus the proton-doped interfacial layer between H-Pt and NNO (i.e., H-NNO) is responsible for the voltage-induced reversible resistive switching.

The asymmetrical device showed clockwise bipolar I-V curves when negative and positive voltage were applied alternatively, regardless of the sweep width ($-2\,V \le V \le 2\,V$ to $-8\,V \le V \le 8\,V$) (Fig. 2(a)). The current ratio between LRS and HRS tended to increase as voltage sweep width increased; this trend means that the volume of the insulating H-NNO layer was controlled by the magnitude of the voltage sweep. By exploiting this voltage-controlled modulation of the insulating layer, the different resistance states of the device could be modulated by consecutively increasing the set voltage in the negative direction and the reset voltage in the positive direction. When set and reset voltages were applied to H-Pt electrodes repeatedly with sweep widths of $-1.0\,V$ to $-9.0\,V$ in the negative direction and $+1.0\,V$ to $+10.0\,V$ in the positive direction, next hysteresis loop appears following the former line (Fig. 2(b)), and resulted in a lower resistance state during negative sweeps and a higher resistance state during positive sweeps, than the former loop (Fig. 2(b), inset). This result indicates that the resistance of the device can be set to a desired value by applying a suitable voltage. This voltage-controlled multi-level switching in our proton-based $NdNiO_3$ memory resistor is suitable for the applications in multi-level computing and potentially neuromorphic devices.

To investigate the potential neuromorphic applications that use protonic resistive switching, iterative small voltage pulses were applied to the device (Fig. 2(c)). The measurement started with 600 potentiating ("set") pulse sequences at first and then the successive 600 depressing ("reset") pulse sequences. Before the analysis, the device was reset to HRS by applying positive voltage sweep. As the number of negative (positive) pulses increased, the conductance increased (decreases), which confirms that the protonic devices show analog synaptic features. The conductance change was not linearly proportional to the number of the pulses: the first increase or decrease of conductance was always the highest, and the conductance tended to saturate with the increased number of pulses during both the potentiating and depressing process. Similar nonlinearity in the potentiating and depressing curves has been reported in other interface-type resistance change random access memory (RRAM)-based synapses.[9,28] Our proton-based synapses also show smooth and monotonic transition between consecutive pulses; this

response is more advantageous for improving the accuracy in neuromorphic systems than typical filamentary RRAM synapses in which pulse-to-pulse conductance fluctuation is large.[29]

The position of the proton in our $NdNiO_3$ lattice appears to be quite stable and the proton-doped $RNiO_3$ films maintains insulating properties even after several days (Fig. S4);[22] these properties are advantageous in nonvolatile memory applications. Based on the retention behavior of insulating H-NNO films, our correlated oxide devices can be expected to show nonvolatile stability of resistance states. Thus, the retention characteristics at HRS formed by positive voltage sweep and at LRS formed by negative voltage sweep were analyzed by reading current during a −0.2 V voltage pulse (Fig. 2(d)). HRS was quite stable (>1000 s) in spite of the small negative voltage pulse which possibly induces LRS, but the current level at LRS decayed logarithmically over time to the HRS after 100 s. This type of current decay at LRS is commonly observed in interface-type resistive switching devices.[30] In our devices, the proton ions that had removed during the set process seem to be easily re-injected into the NNO layers near the interface during the retention test at LRS; this process may be the cause for the slow decay of LRS to HRS.

As mentioned before, our device shows the distinct clockwise resistive switching, which is in the direction opposite to that of representative interfacial resistive switching heterostructures (e.g., Pt/Nb-doped $SrTiO_3$). In Pt/Nb-doped $SrTiO_3$, the origin of the resistive switching mechanism has long been debated and various models have been proposed, such as charge trapping/detrapping of charge carriers at the interface states[30,31] and modification of electronic structures at the interface as a consequence of electro-migration of oxygen ions (or vacancies).[32,33] Although numerous mechanisms to explain the resistive switching in Pt/Nb-doped $SrTiO_3$ systems have been suggested, the consensus is that oxygen vacancies (or interface states induced by oxygen-related defects) contribute to the change of resistance. Due to the migration of negative ions, this interface-type resistive switching shows counter-clockwise sweep when voltage bias is applied to the top electrodes near the highly insulating depletion layer; Unlike other memristors, the opposite response occurs in our asymmetrical devices, so that oxygen-related defects are unlikely to be the origin of our resistive switching.

Based on our distinct IV characteristics, proton in NNO lattice is attributed into the origin of the resistive switching in our devices. One likely scenario of the origin is that asymmetrical proton concentration between the two electrodes is modulated by externally applied bias as a result of the migration of proton (Fig. 1(b)). A high resistance layer (H-NNO) forms in the NNO layer under the H-Pt electrode by selectively introducing proton due to the catalytic effect of the Pt; the HRS results. When a negative voltage bias is applied on H-Pt (i.e., "set" process), protons in the NNO layer migrate toward the H-Pt electrode and thus reduce the effective thickness of the insulating layer (H-NNO); the LRS ensues. Subsequent application of positive bias to the H-Pt electrodes reversibly pushes the proton back to the NNO layer, the H-NNO layer with high resistance re-forms, and the HRS is re-established. In this model, the H-Pt electrodes seem to act as proton reservoirs to supply proton into the H-NNO layers during the reset process and to remove the proton from the H-NNO layers during the set process.

To experimentally verify the asymmetrical distribution of proton in the NNO film underneath each Pt electrode, dynamic secondary ion mass spectroscopy (D-SIMS, IMS 4FE7) was performed at two positions of Pt electrodes with different process histories, i.e., NH-Pt and H-Pt, to detect the hydrogen ions in the NNO films. Depth profiling of the chemical composition was analyzed using D-SIMS under the NH-Pt and H-Pt electrodes, respectively, as shown in Fig. 3. Hydrogen concentration in NNO layer underneath NH-Pt was similar to that of background (Fig. 3(a)), whereas large amount of hydrogen, whose concentration is two orders of magnitude greater than the background concentration, was detected in NNO layer underneath H-Pt (Fig. 3(b)). The results suggest that the proton ion is actually intercalated into the NNO lattice and induces the local transition of NNO from conductor to insulator under the H-Pt electrode after the hydrogenation process. Considering the low mass and small ionic radius of proton, our suggested models are plausible. Furthermore, in solid oxide electrolytes, the proton conductivity is usually higher than oxygen ion conductivity,[34] so our devices should be appropriate for low-power operation. Therefore, because of the greater ease of proton migration in transition metal oxides, our protonic memory resistors may overcome the limitations of oxygen-based resistive switching devices and create new paradigm for the future application of neuromorphic devices.[35]

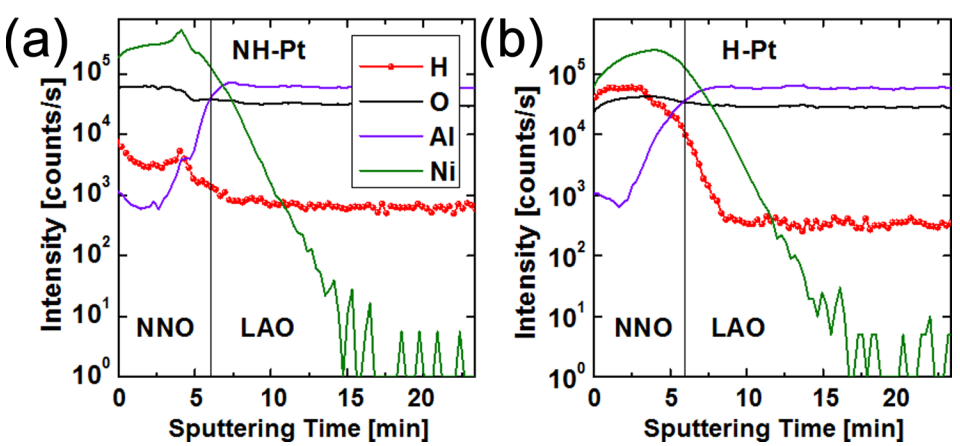

FIG. 3. Dynamic secondary ion mass spectroscopy (D-SIMS) depth profiles of hydrogen (H), oxygen (O), aluminum (Al), and nickel (Ni) in our protonic memory resistors at the vertical direction of (a) NH-Pt electrode and (b) H-Pt electrode.

In summary, we have realized proton-based memory resistors with multilevel states in epitaxial NNO heterostructure devices by designing the asymmetry of proton concentration. Due to the extreme sensitivity of NNO resistivity to proton, switching occurs near the hydrogenated interface, and the extent of resistance modulation in our protonic devices can be controlled by adjusting the magnitude of the external bias. Exploitation of resistive switching by proton migration in correlated oxides provides a strategy to design energy-efficient electronic devices by overcoming the fundamental bottleneck conventional resistive switching devices, and provides an important step toward the development of correlated electronics, such as two-terminal neuromorphic devices.

The authors gratefully acknowledge Kyuwook Ihm for his help in XAS measurement. This work was supported by Basic Science Research Program through the National Research Foundation of Korea (NRF) funded by the Ministry of Science, ICT and Future Planning (2014R1A1A1035950) and the IT R&D program of MOTIE/KEIT (10045226).

[1]M. Imada, A. Fujimori, and Y. Tokura, Rev. Mod. Phys. **70**, 1039 (1998).
[2]S. Stemmer and A. J. Millis, MRS Bull. **38**, 1032–1039 (2013).
[3]Z. Yang, C. Ko, and S. Ramanathan, Annu. Rev. Mater. Res. **41**, 337–367 (2011).
[4]F. Chudnovskiy, S. Luryi, and B. Spivak, "Switching device based on first-order metal-insulator transition induced by external electric field," in *Future Trends in Microelectronics: The Nano Millennium*, edited by S. Luryi, J. M. Xu, and A. Zaslavsky (Wiley Interscience, 2002), pp. 148–155.
[5]J. H. Ngai, F. J. Walker, and C. H. Ahn, Annu. Rev. Mater. Res. **44**, 1–17 (2014).
[6]J. Son, S. Rajan, S. Stemmer, and S. James Allen, J. Appl. Phys. **110**, 084503 (2011).
[7]M. Nakano, K. Shibuya, D. Okuyama, T. Hatano, S. Ono, M. Kawasaki, Y. Iwasa, and Y. Tokura, Nature **487**, 459–462 (2012).
[8]J. Jeong, N. Aetukuri, T. Graf, T. D. Schladt, M. G. Samant, and S. S. P. Parkin, Science **339**, 1402–1405 (2013).
[9]J. Shi, S. D. Ha, Y. Zhou, F. Schoofs, and S. Ramanathan, Nat. Commun. **4**, 2676 (2013).
[10]N. Shukla, A. V. Thathachary, A. Agrawal, H. Paik, A. Aziz, D. G. Schlom, S. K. Gupta, R. Engel-Herbert, and S. Datta, Nat. Commun. **6**, 7812 (2015).
[11]J. B. Torrance, P. Lacorre, A. I. Nazzal, E. J. Ansaldo, and C. Niedermayer, Phys. Rev. B **45**, 8209–8212 (1992).
[12]J. Son, P. Moetakef, J. M. LeBeau, D. Ouellette, L. Balents, S. J. Allen, and S. Stemmer, Appl. Phys. Lett. **96**, 062114 (2010).
[13]D. G. Ouellette, S. Lee, J. Son, S. Stemmer, L. Balents, A. J. Millis, and S. J. Allen, Phys. Rev. B **82**, 165112 (2010).
[14]P. C. Canfield, J. D. Thompson, S. W. Cheong, and L. W. Rupp, Phys. Rev. B **47**, 12357–12360 (1993).
[15]J. S. Zhou, J. B. Goodenough, and B. Dabrowski, Phys. Rev. Lett. **94**, 226602 (2005).
[16]J. Son, J. M. LeBeau, S. J. Allen, and S. Stemmer, Appl. Phys. Lett. **97**, 202109 (2010).
[17]A. V. Boris, Y. Matiks, E. Benckiser, A. Frano, P. Popovich, V. Hinkov, P. Wochner, M. Castro-Colin, E. Detemple, V. K. Malik, C. Bernhard, T. Prokscha, A. Suter, Z. Salman, E. Morenzoni, G. Cristiani, H. U. Habermeier, and B. Keimer, Science **332**, 937–940 (2011).
[18]A. J. Hauser, E. Mikheev, N. E. Moreno, J. Hwang, J. Y. Zhang, and S. Stemmer, Appl. Phys. Lett. **106**, 092104 (2015).
[19]S. D. Ha, M. Otaki, R. Jaramillo, A. Podpirka, and S. Ramanathan, J. Solid State Chem. **190**, 233–237 (2012).
[20]S. Asanuma, P. H. Xiang, H. Yamada, H. Sato, I. H. Inoue, H. Akoh, A. Sawa, K. Ueno, H. Shimotani, H. Yuan, M. Kawasaki, and Y. Iwasa, Appl. Phys. Lett. **97**, 142110 (2010).
[21]R. Scherwitzl, P. Zubko, I. G. Lezama, S. Ono, A. F. Morpurgo, G. Catalan, and J. M. Triscone, Adv. Mater. **22**, 5517–5520 (2010).
[22]J. Shi, Y. Zhou, and S. Ramanathan, Nat. Commun. **5**, 4860 (2014).
[23]J. K. Chen, Y. Zhou, S. Middey, J. Jiang, N. F. Chen, L. D. Chen, X. Shi, M. Dobeli, J. Shi, J. Chakhalian, and S. Ramanathan, Appl. Phys. Lett. **107**, 031905 (2015).
[24]J. Son, B. Jalan, A. P. Kajdos, L. Balents, S. James Allen, and S. Stemmer, Appl. Phys. Lett. **99**, 192107 (2011).
[25]See supplementary material at http://dx.doi.org/10.1063/1.4944842 for structural properties, electrical properties of epitaxial thin films, retention behavior and XAS characterization.
[26]T.-J. Chu, T.-M. Tsai, T.-C. Chang, K.-C. Chang, R. Zhang, K.-H. Chen, J.-H. Chen, T.-F. Young, J.-W. Huang, J.-C. Lou, M.-C. Chen, S.-Y. Huang, H.-L. Chen, Y.-E. Syu, D. Bao, and S. M. Life, IEEE Electron Device Lett. **35**, 217–219 (2014).
[27]A. Hanada, K. Kinoshita, and S. Kishida, Appl. Phys. Lett. **101**, 043507 (2012).
[28]Y. F. Wang, Y. C. Lin, I. T. Wang, T. P. Lin, and T. H. Hou, Sci. Rep. **5**, 10150 (2015).
[29]S. Mandal, A. El-Amin, K. Alexander, B. Rajendran, and R. Jha, Sci. Rep. **4**, 5333 (2014).
[30]E. Mikheev, B. D. Hoskins, D. B. Strukov, and S. Stemmer, Nat. Commun. **5**, 3990 (2014).
[31]J. Park, D.-H. Kwon, H. Park, C. U. Jung, and M. Kim, Appl. Phys. Lett. **105**, 183103 (2014).
[32]M. Janousch, G. I. Meijer, U. Staub, B. Delley, S. F. Karg, and B. P. Andreasson, Adv. Mater. **19**, 2232–2235 (2007).
[33]D.-J. Seong, M. Jo, D. Lee, and H. Hwang, Electrochem. Solid-State Lett. **10**, H168 (2007).
[34]K. D. Kreuer, Annu. Rev. Mater. Res. **33**, 333–359 (2003).
[35]E. E. Josberger, Y. Deng, W. Sun, R. Kautz, and M. Rolandi, Adv. Mater. **26**, 4986–4990 (2014).